Pacific Symposium on Biocomputing 12:181-192(2007)

COMPARATIVE METABOLOMICS OF BREAST CANCER*

CHEN YANG†, ADAM D. RICHARDSON†,
JEFFREY W. SMITH, and ANDREI OSTERMAN
The Burnham Institute for Medical Research,
La Jolla, California 92037, USA

Comparative metabolic profiling of cancerous and normal cells improves our understanding of the fundamental mechanisms of tumorigenesis and opens new opportunities in target and drug discovery. Here we report a novel methodology of comparative metabolome analysis integrating the information about both metabolite pools and fluxes associated with a large number of key metabolic pathways in model cancer and normal cell lines. The data were acquired using [U-^{13}C]glucose labeling followed by two-dimensional NMR and GC-MS techniques and analyzed using isotopomer modeling approach. Significant differences revealed between breast cancer and normal human mammary epithelial cell lines are consistent with previously reported phenomena such as upregulation of fatty acid synthesis. Additional changes established for the first time in this study expand a remarkable picture of global metabolic rewiring associated with tumorigenesis and point to new potential diagnostic and therapeutic targets.

1. Introduction

Since the completion the human genome, the main thrust of functional genomics has been to establish the link between gene/protein expression profiles and cellular phenotype in normal and disease states, most notably in cancer. Remarkable advancements in transcriptomics and proteomics technologies (1,2) led to the identification of novel therapeutic targets as well as tumor subtypes and biomarkers (3-6). Nevertheless, these technologies, taken alone, fall short of reflecting the entire picture of cellular networks and pathways. A direct assessment of a large number of intermediary metabolites and metabolic activities (metabolomics) is emerging as a powerful complementary approach for identifying pathways that are perturbed in a given pathology. Metabolic profiling is of special importance in cancer biology due to profound changes in central metabolism associated with many tumors as established by early biochemical studies (7) and recently confirmed by functional genomics techniques. Nevertheless, our current knowledge of the molecular processes associated with these metabolic changes is quite incomplete.

* This work was partially supported by a California Breast Cancer Research Program Fellowship to CY and by the Burnham Institute Cancer Center Support Grant (2 P30 CA30199-24, PI R. Abraham).
† Both authors contributed equally to this work.

Despite the recent progress in metabolomics technology its applications in the field of human biology are still limited, mostly due to many technical challenges. Among the most obvious are: a limited availability of biological material, insufficient sensitivity and resolution of existing protocols, incomplete reference data (eg for NMR peak assignment) and the lack of established computational modeling framework. In this study we addressed some of these problems by combining [U-^{13}C]-glucose labeling with two-dimensional NMR and GC-MS techniques to assess simultaneously the metabolite pools and fluxes associated with several interrelated metabolic pathways in human cells. We were able to assign two-dimensional NMR signals for 24 intermediary metabolites representing a substantial fraction of central metabolism. The acquired data were analyzed using an isotopomer model derived from reconstruction of an extensive metabolic network.

We applied this approach for the **comparative analysis** of breast cancer and normal human mammary epithelial cell lines. An isotopomer model was developed for a metabolic network including the reactions of central carbon, fatty acid, and amino acid metabolism. We chose this metabolic network because it is the central backbone of metabolism providing energy, cofactor regeneration, and building blocks for cell synthesis. Moreover, cancer cells have been reported to display different activities of some of these pathways. We determined the active pathways and the flux distribution in this metabolic network. The observed pattern of metabolic changes is consistent with earlier observations of metabolic shifts in tumors (7), validating the developed methodology. A number of newly established changes in metabolic fluxes and pools provided us with new insights to potential diagnostic markers and therapeutic targets.

2. Materials and Methods

2.1 Experimental techniques

Experimental procedures are only briefly introduced in this subsection. The details are provided in the Supplementary on-line Materials (SOM) [1].

Cell lines and cultivation. Human cell lines used in this study were: MCF-10A (ATCC), derived from normal mammary epithelial cells, and MDA-MB-435 (NCI), a highly metastatic mammary epithelial cancer cell line. Cultivation, metabolic labeling with 20% [U-^{13}C]glucose and harvesting was performed as described in SOM.

[1] available at: http://www.burnham.org/labs/osterman/

Gas Chromatography – Mass Spectrometry (GC-MS) was used to analyze fatty acids. Samples from ~ 5×10^7 cells were prepared as described (8) and analyzed on Trace GC/Trace MS Plus system (see SOM for details). Mass isotopomer distribution corrected for natural abundance (9), was used to assess de novo fatty acid synthesis as described (8).

Nuclear Magnetic Resonance (NMR) was used to analyze a mixture of methanol- and water-soluble metabolites extracted from ~ 2.5×10^8 labeled cells as described in SOM. Two-dimensional [^{13}C,^{1}H] HSQC spectra were acquired using a Bruker Avance 500 NMR spectrometer. The ^{13}C-^{13}C scalar coupling fine structures were extracted from the cross sections taken along the ^{13}C axis in a HSQC spectrum by using the Bruker XWINNMR software. The concentrations of metabolites were determined by integrating the cross peaks in the HSQC spectra using the NMRPipe (10) and Sparky (http://www.cgl.ucsf.edu/home/sparky/) software packages, comparing with the integral of resonances peaks of the L-methionine that was treated as an internal standard, and normalizing to the amount of total cellular protein.

2.2. ^{13}C- Isotopomer Model

A mathematical model describing the ^{13}C isotopomer distribution of metabolites in human cells fed with ^{13}C-glucose was developed. It was used for the determination of metabolic fluxes using ^{13}C-multiplet patterns of metabolites from HSQC spectra. The considered metabolic network included glycolysis, pentose phosphate pathway (PPP), tricarboxylic acid (TCA) cycle, anaplerotic reaction, and biosynthetic pathways of fatty acids and non-essential amino acids. The fraction of de novo synthesis of fatty acids was determined based on the mass isotopomer distribution measured by GC-MS as described (8). The fluxes through other pathways are derived as follows.

Contribution of PPP to pyruvate/alanine formation. The assessment of PPP activity relies on the analysis of ^{13}C multiplets of alanine C2. The observed relative multiplet intensities were transformed to the relative abundances of intact carbon fragments (11). According to the carbon rearrangements in PPP, three pentose molecules (C1-C2-C3-C4-C5 backbone) yield five pyruvate molecules. Three of them retain an intact C1-C2-C3 fragment, while two molecules carry only a C2-C3 fragment of the original backbone. The latter fraction denoted as $f^{(2)}$(Ala-C2), is the main contributor to the isotopomer population of [2,3-$^{13}C_2$]alanine as assessed by the relative intensity of the doublet ($^{1}J_{CC}$ = 35 Hz) of alanine C2. The total fraction of pyruvate derived from PPP can be estimated as $5/2 * f^{(2)}$(Ala-C2).

TCA cycle and anaplerotic flux. [U-^{13}C]pyruvate enters the TCA cycle either by pyruvate dehydrogenase oxidation or by the anaplerotic reaction of

pyruvate carboxylase. The first process generates [4,5-$^{13}C_2$]α-ketoglutarate via [1,2-$^{13}C_2$]acetyl-CoA. Since intracellular α-ketoglutarate concentration is too low to be detected by NMR, its labeling state was assessed via glutamate, an abundant metabolite in rapid exchange with α-ketoglutarate. The isotopomer population of [4,5-$^{13}C_2$]glutamate reflects the flux through pyruvate dehydrogenase, which equals the TCA cycle (citrate synthase) flux, provided the acetyl-CoA synthetase flux is zero. The second process is expected to yield a distinct labeling pattern represented by [1,2,3-$^{13}C_3$] and [2,3-$^{13}C_2$] glutamate. This pattern reflects the formation of [1,2,3-$^{13}C_3$] and [2,3,4-$^{13}C_3$] oxaloacetate due to the pyruvate carboxylase reaction followed by the reversible interconversion between the asymmetric oxaloacetate and symmetric succinate (or fumarate). The relative activity of pyruvate carboxylase versus pyruvate dehydrogenase (v_{PC} / v_{PDH}) was calculated from the ^{13}C multiplet components of glutamate at C3 and C4 using Eq. 1:

$$\frac{v_{PC}}{v_{PDH}} = \frac{d(\text{Glu}-\text{C3})}{d^{*}(\text{Glu}-\text{C4}) + q(\text{Glu}-\text{C4})} \qquad (1)$$

where d(Glu-C3) is the contribution of doublet ($^1J_{CC}$ = 35 Hz) to the multiplets of glutamate C3, while d*(Glu-C4) and q(Glu-C4) are the relative contributions of the doublet with $^1J_{CC}$ coupling constant of 55 Hz and the quartet to the glutamate C4 multiplets, respectively.

Non-essential amino acid biosynthesis. We investigated the activities of biosynthetic pathways of cysteine, glutamate, glutamine, glycine, and proline. The equation used for glycine biosynthesis is derived as follows, similarly for the other amino acids. Glycine can be synthesized via serine from the glycolytic intermediate, 3-phosphoglycerate, or obtained directly from media components. 3-Phosphoglycerate has the same labeling pattern as pyruvate. Thus we obtain the isotopomer balance equation (2).

$$P_{\text{Gly}-\text{C2}} \cdot \begin{bmatrix} s \\ d \end{bmatrix}_{\text{Gly}-\text{C2}} = X^{\text{syn}} \cdot P_{\text{Ala}-\text{C2}} \cdot \begin{bmatrix} s+d \\ d^{*}+q \end{bmatrix}_{\text{Ala}-\text{C2}} + (1-X^{\text{syn}}) \cdot P_n \cdot \begin{bmatrix} 1-P_n \\ P_n \end{bmatrix} \qquad (2)$$

where X^{syn} is the fraction of glycine derived from glycolysis; s, d, d*, and q correspond to the relative intensities of singlet, doublet, doublet with a larger coupling constant and quartet, respectively. P_n is the natural ^{13}C abundance (P_n = 0.011), and $P_{Gly\text{-}C2}$ and $P_{Ala\text{-}C2}$ are the specific enrichments of glycine C2 and alanine C2. $P_{Gly\text{-}C2}$ can be calculated from X^{syn}, P_n and $P_{Ala\text{-}C2}$ using the relation $P_{Gly\text{-}C2} = X^{syn} \cdot P_{Ala\text{-}C2} + (1 - X^{syn}) \cdot P_n$. Therefore X^{syn} can be derived from the analysis of ^{13}C multiplets of alanine C2 and glycine C2 using Eq. 3:

$$X^{\text{syn}} = \frac{P_n \cdot \left(\begin{bmatrix} s \\ d \end{bmatrix}_{\text{Gly-C2}} - \begin{bmatrix} 1-P_n \\ P_n \end{bmatrix}\right)}{P_{\text{Ala-C2}} \cdot \left(\begin{bmatrix} s+d \\ d*+q \end{bmatrix}_{\text{Ala-C2}} - \begin{bmatrix} s \\ d \end{bmatrix}_{\text{Gly-C2}}\right) + P_n \cdot \left(\begin{bmatrix} s \\ d \end{bmatrix}_{\text{Gly-C2}} - \begin{bmatrix} 1-P_n \\ P_n \end{bmatrix}\right)} \quad (3)$$

3. Results

3.1. NMR Spectral Assignment

Fig. 1 shows a typical two-dimensional [^{13}C,^{1}H] HSQC spectrum of metabolites extracted from the human breast cancer cells. The assignment of ^{13}C-^{1}H cross peaks for various metabolites was made by comparing the carbon and proton chemical shifts with literature values (12-17), with spectra of pure compounds and by spiking the samples. Overall, 24 metabolites could be unambiguously assigned. The details of peak assignments and the reference summary Table S1 of characteristic chemical shifts are provided in SOM.

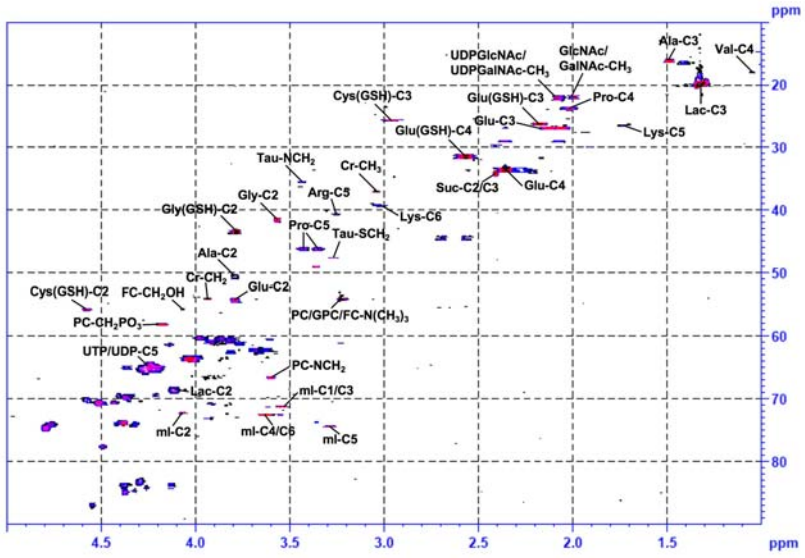

Fig. 1. A typical two-dimensional [^{13}C, ^{1}H] HSQC spectrum of the metabolites extracted from breast cancer cells. Abbreviations for the assigned peaks are as in Table S1.

3.2. Metabolic Fluxes

A comparison of relative intensities of ^{13}C-^{13}C scalar coupling multiplet components of various metabolites extracted from [U-^{13}C]glucose labeled MCF-

10A and MDA-MB-435 cells are shown in Table 1. These data were used in the ^{13}C isotopomer model to determine the metabolic fluxes or flux ratios through individual pathways including glycolysis, PPP, TCA cycle and anaplerotic reaction, fatty acid and amino acid biosynthetic pathways (Fig. 2).

Table 1. Relative intensities of ^{13}C multiplet components of metabolites extracted from MCF-10A and MDA-MB-435 cells grown on [U-^{13}C]glucose [a]

Carbon position	Isotopomer populations	Multiplet components	MCF-10A	MDA-MB-435
Alanine-C2	2-^{13}C	s	0.27	0.16
	2,3-$^{13}C_2$	d	0.01	0.11
	1,2-$^{13}C_2$	d*	0.01	0.01
	1,2,3-$^{13}C_3$	q	0.71	0.72
Alanine-C3	3-^{13}C	s	0.28	0.17
	2,3-$^{13}C_2$	d	0.72	0.83
Lactate-C3	3-^{13}C	s	0.16	0.20
	2,3-$^{13}C_2$	d	0.84	0.80
Acetyl-CoA (GlcNAc/GalNAc)-C2	2-^{13}C	s	0.29	0.14
	1,2-$^{13}C_2$	d	0.71	0.86
Glutamine-C4	4-^{13}C	s	0.50	–[b]
	3,4-$^{13}C_2$	d	0.01	–[b]
	4,5-$^{13}C_2$	d*	0.48	–[b]
	3,4,5-$^{13}C_3$	q	0.01	–[b]
Glutamate-C3	3-^{13}C	s	0.73	0.72
	2,3-$^{13}C_2$ / 3,4-$^{13}C_2$	d	0.27	0.27
	2,3,4-$^{13}C_3$	t	0	0.01
Glutamate-C4	4-^{13}C	s	0.50	0.30
	3,4-$^{13}C_2$	d	0.01	0.01
	4,5-$^{13}C_2$	d*	0.48	0.66
	3,4,5-$^{13}C_3$	q	0.01	0.03
Glu (GSH)-C3	3-^{13}C	s	0.67	0.71
	2,3-$^{13}C_2$ / 3,4-$^{13}C_2$	d	0.32	0.28
	2,3,4-$^{13}C_3$	t	0.01	0.01
Glu (GSH)-C4	4-^{13}C	s	0.24	0.13
	3,4-$^{13}C_2$	d	0.02	0.02
	4,5-$^{13}C_2$	d*	0.70	0.73
	3,4,5-$^{13}C_3$	q	0.04	0.12
Gly (GSH)-C2	2-^{13}C	s	0.88	0.27
	1,2-$^{13}C_2$	d	0.12	0.73
Glycine-C2	2-^{13}C	s	0.86	0.27
	1,2-$^{13}C_2$	d	0.14	0.73
Proline-C4	4-^{13}C	s	1.00	0.25
	4,5-$^{13}C_2$	d	0.00	0.71
	3,4,5-$^{13}C_3$	t	0.00	0.04
Proline-C5	5-^{13}C	s	1.00	0.25
	4,5-$^{13}C_2$	d	0.00	0.75

[a] s, singlet; d, doublet (^1Jcc, ~35 Hz); d*, doublet split by a large coupling constant (^1Jcc, ~60 Hz); t, triplet; q, quartet.
[b] Resonance of glutamine C4 is below the detection level in the MDA-MB-435 cells.

The relative activity of PPP versus glycolysis was determined based on the analysis of ^{13}C multiplets of alanine C2 as described above. The contribution of

the signature doublet ($^1J_{CC}$ = 35 Hz) to the multiplets of alanine C2 is very small in MCF-10A but significant in MDA-MB-435 cells (Table 1), suggesting that a relative contribution of PPP to production of pyruvate is substantially higher in malignant cells (28%) compared to nonmalignant cells (~2%), where the bulk of pyruvate stems from glycolysis (Fig. 2). The increased use of PPP enables the MDA-MB-435 cells not only to supply more ribose for nucleic acid synthesis, but to recruit more of the NADPH reducing power for fatty acid synthesis. Indeed, the GC/MS analysis performed in this study revealed that 47% of palmitate is newly synthesized from glucose in MDA-MB-435 cells (Fig. 2) in correlation with the observed increase in PPP flux. The de novo synthesized palmitoleate, stearate, and oleate is 37%, 35%, and 18%, respectively. This is in marked contrast with almost no *de novo* fatty acid synthesis in MCF-10A cells as evidenced by the lack of ^{13}C tracer accumulation in palmitate, palmitoleate, stearate or oleate.

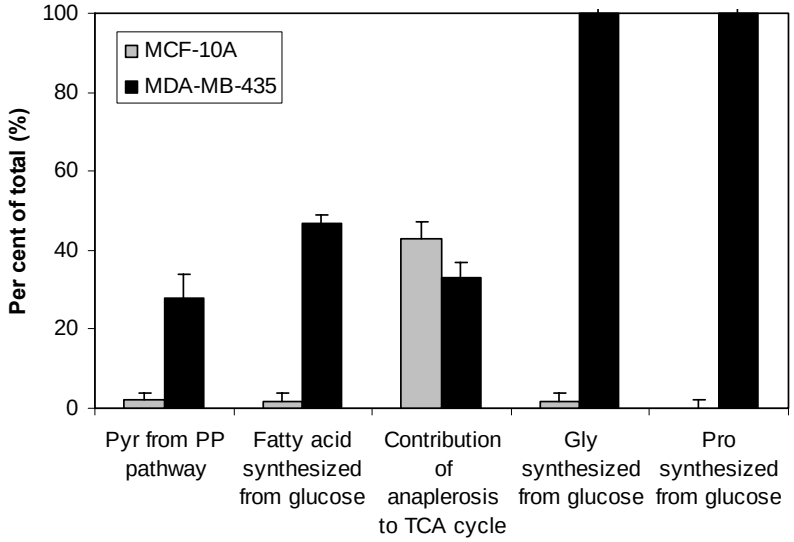

Fig. 2. Metabolic fluxes in MCF-10A and MDA-MB-435 cells (mean + s.d.; *n*=4).

The relative fluxes through pyruvate carboxylase and pyruvate dehydrogenase were estimated from the analysis of glutamate labeling. The major isotopomer populations of 4,5-$^{13}C_2$ of glutamate and γ-glutamyl of glutathione indicated that these carbon atoms are derived from [1,2-$^{13}C_2$]acetyl-CoA (Table 1). The isotopomer ratio of acetyl-CoA C2, 1,2-$^{13}C_2$ / 2-$^{13}C_1$, which can be assessed via the acetyl moiety of GlcNAc or GalNAc, is 2.5 for MCF-10A and 6.1 for MDA-MB-435. Whereas these ratios are similar to the isotopomer ratios of 4,5-$^{13}C_2$ + 3,4,5-$^{13}C_3$ / 4-$^{13}C_1$ + 3,4-$^{13}C_2$ of glutathione C4

(2.8 for MCF-10A and 5.7 for MDA-MB-435), they are markedly different from the glutamate C4 ratios (0.96 for MCF-10A and 2.2 for MDA-MB-435). This indicates that the C4 and C5 in the γ-glutamyl moiety of glutathione are solely derived from acetyl-CoA, whereas glutamate is a likely subject of the isotopic dilution originating from a non-enriched carbon source (e.g. glutamine). Therefore, the isotopomer distribution of γ-glutamyl of glutathione was used to determine the relative activity of the anaplerotic reaction versus TCA cycle. The observed flux ratio of pyruvate carboxylase reaction over TCA cycle is slightly decreased in MDA-MB-435 compared to MCF-10A cells (Fig.2).

Analysis of the ^{13}C labeling pattern of the nonessential amino acids allowed us to determine the activity of the respective biosynthetic pathways. Using the ^{13}C isotopomer model, we found that cysteine is obtained directly from media components, and the activity of glutamate and glutamine biosynthesis is not changed significantly in MCF-10A and MDA-MB-435 cells (data not shown). Interestingly, MCF-10A cells do not utilize glucose for synthesis of glycine and proline, whereas these amino acids are actively synthesized from glucose in MDA-MB-435 cells (Fig. 2).

3.3. Metabolite Pools

We used the 2D NMR data from the same labeling experiments to determine and compare the concentrations of unambiguously assigned metabolites (Table 2). Quantitation of metabolites with natural isotope abundance yields directly the total metabolite concentrations. At the same time, the differences observed for biosynthetically labeled metabolites may originate from changes in pool sizes as well as due to the ^{13}C enrichment. In many cases these effects can be decoupled as illustrated below.

Comparison of MCF-10A and MDA-MB-435 cell lines revealed significant changes in the pool sizes of many metabolites. For example, malignant cells exhibited significantly increased glutathione, *m*-inositol, and creatine concentrations and decreased isoleucine, leucine, valine, and taurine concentrations. Phosphocholine level is higher, whereas free choline and glycerophosphocholine were below the detection level in MDA-MB-435.

The observed 12-fold increase in C2 and C3 peaks of succinate may not be explained solely by the ^{13}C enrichment, which could account only for ~12% of the overall increase. The latter estimate is based on the labeling pattern of α-ketoglutarate deduced from the observed ~1.3-fold ^{13}C enrichment at the C3 and C4 of γ-glutamyl moiety of glutathione. Therefore, the total pool size of succinate was significantly increased in MDA-MB-435 cells. A similar approach allowed us to establish a substantial increase in the total pool size of GlcNAc or GalNAc and a decrease in those of alanine, glutamine, and glycine (Fig.3).

Table 2. Comparison of metabolite concentrations in MCF-10A and MDA-MB-435 cells [a]

Metabolites [b]	Ratio MDA-MB-435 / MCF-10A	Metabolites labeled at specific positions [c]	Ratio MDA-MB-435 / MCF-10A
Arginine	0.98 ± 0.15	Alanine C2	1.02 ± 0.05
GSH	1.59 ± 0.08	Alanine C3	1.00 ± 0.05
Isoleucine	0.27 ± 0.04	Glutamine C4	< 0.05
Leucine	0.48 ± 0.05	Glutamate C3	1.56 ± 0.22
Lysine	0.74 ± 0.16	Glutamate C4	2.09 ± 0.31
Valine	0.26 ± 0.03	Glu (GSH) C3	2.17 ± 0.16
m-Inositol	1.75 ± 0.10	Glu (GSH) C4	1.94 ± 0.15
Free choline	< 0.25	Gly (GSH) C2	6.54 ± 0.98
Phosphocholine	1.72 ± 0.09	Glycine C2	1.15 ± 0.06
Glycerophosphocholine	< 0.10	Proline C4	8.57 ± 2.53
Total choline	1.39 ± 0.17	Proline C5	10.9 ± 3.3
Phosphocholine / glycerophosphocholine	> 17.2	Lactate C2	0.67 ± 0.17
Creatine	1.74 ± 0.08	Succinate C2/C3	> 12.3
Taurine	0.25 ± 0.03	GlcNAc / GalNAc C2	> 14.7
		UDP-GlcNAc / UDP-GalNAc C2	2.56 ± 0.64
		UTP / UDP C1	3.38 ± 0.53

[a] Relative amount of the various compounds were obtained by normalizing peaks to the internal reference standard, and further normalized per 1 mg of total protein (mean + s.d.; *n*=4)
[b] Quantitation of metabolites with natural isotope abundance (a direct measure of metabolite concentrations).
[c] Differences observed for biosynthetically labeled metabolites may reflect both, a ^{13}C enrichment and a change in a total pool size.

4. Discussion

The key aspects of the metabolomics methodology used in this study were:

1**. A comparative approach** was applied to assess metabolic changes in a model system of the highly metastatic cell line MDA-MB-435 versus the immortalized nontumorigenic cell line MCF-10A.

2. **[U-^{13}C]glucose labeling followed by the high-resolution 2D NMR** spectroscopy allowed us to monitor twenty-four intracellular metabolites (Tables 1 and 2) in addition to fatty acids analyzed by GC-MS.

3. **An extensive ^{13}C isotopomer model** was developed to determine and compare fluxes through the key central metabolic pathways including glycolysis, PPP, TCA cycle and anaplerotic reactions, and biosynthetic pathways of fatty acids and non-essential amino acids (Fig.2).

4. **A combination of fluxes with individual metabolite pools** within the single metabolic reconstruction framework expanded our ability to interpret underlying metabolic transitions (Fig.3).

Although most of the individual components of this approach have been previously described, to our knowledge this is the first study when a combination of these techniques was systematically applied for metabolomics of

cancer. Although comprehensive isotopomer models are widely used in microbial systems (18,19), only a few models have been described for human cells (20-29). Most of these models were restricted by relatively narrow metabolic subnetworks (20-25) or based on the labeling data for one (i.e. glutamate (25,26)) or a few individual metabolites (27-29). Due to the higher sensitivity of HSQC method compared to regular ^{13}C-NMR we were able to decrease the amount of cells required for the analysis. The increased signal dispersion in 2D spectra allowed us to analyze a wide range of metabolites without prior separation.

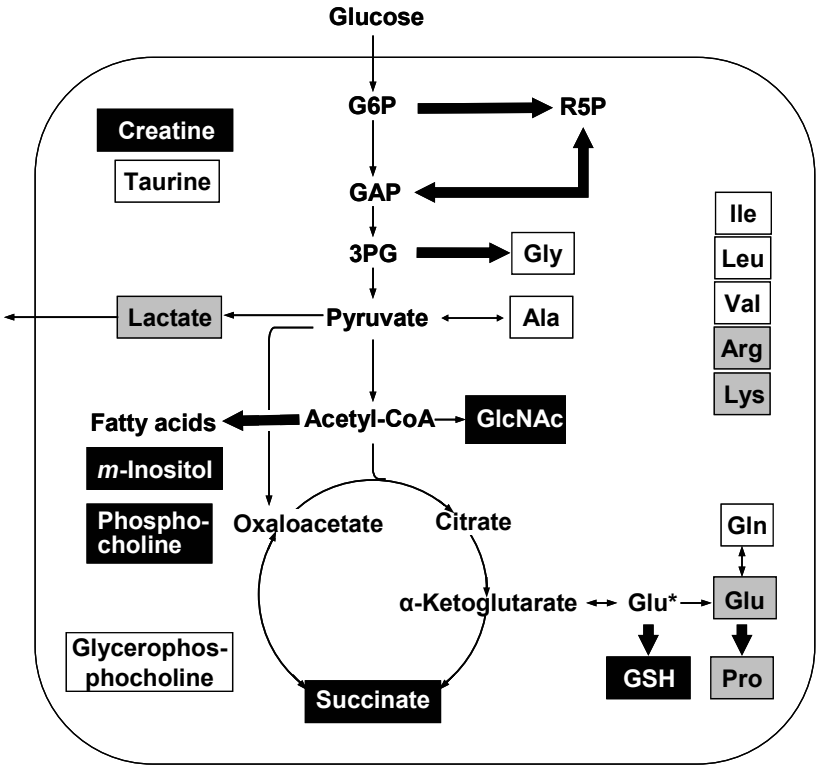

Fig. 3. Metabolic profile changes in breast tumors compared with normal human mammary epithelial cells. The arrows represent the fluxes. Fluxes are normalized to glucose uptake rate. The boldface arrows indicate the fluxes that are significantly upregulated. The pool sizes of boxed metabolites are directly assessed by [^{13}C,^{1}H] HSQC. Metabolites are colored if their concentrations are increased (black), decreased (white), or not changed (gray). G6P, glucose-6-phosphate; R5P, ribose-5-phosphate; GAP, glyceraldehydes-3-phosphate; 3-PG, 3-phosphoglycerate. See other abbreviations in Table S1 given in SOM.

An integration of fluxes and pool sizes acquired within a single experiment

gives a more detailed fingerprint of the phenotype compared to conventional approaches based on one parameter. Although fluxes provide a direct measure of metabolic activities pointing to potential targets, they can be usually obtained only for a subset of central metabolic pathways. Metabolite pools can be readily assessed for both central and peripheral metabolites. While providing only an indirect evidence of metabolic activities, they can be used as biomarkers.

We observed a sharp increase in metabolic activity of several pathways in cancer cells (Fig.2 and 3). Some of these observations such as upregulation of PPP and fatty acid synthesis are consistent with previous reports (30,31) providing us with a validation of the approach. An increase in other fluxes, eg the synthesis of glycine and proline, are reported here for the first time. Possible implications of these changes in establishing and maintaining a breast cancer phenotype are yet to be explored. Some of the observed changes in metabolite pools can be readily interpreted in the context of respective fluxes. For example the pools of all monitored amino acids decreased or remained largely unchanged in cancer cells, despite the established upregulation of some of the respective biosynthetic pathways (Fig.3). This is consistent with accelerated consumption of amino acids for protein synthesis. At the same time, the pool of glutathione (GSH in Fig.3), which is not consumed at the same level increased in keeping with the increased synthetic flux. Overproduction of GSH in tumors may reflect the increased resistance towards oxidative stress (32). We observed significant alterations in pools of several peripheral metabolites (eg creatine and taurine), whose metabolism may not be easily assessed via flux measurements.

Therefore, the results obtained in this study, in addition to the validation of the approach, provide new information about metabolic aspects of tumorigenesis, and can aid the identification of new diagnostic and therapeutic targets. The presented approach constitutes a promising analytical tool to screen different metabolic phenotypes in a variety of cell types and pathological conditions.

REFERENCES

1. Chu, S., DeRisi, J., Eisen, M., Mulholland, J., Botstein, D., Brown, P. O., and Herskowitz, I. (1998) *Science* **282**, 699-705
2. Klose, J., Nock, C., Herrmann, M., Stuhler, K., Marcus, K., Bluggel, M., Krause, E., Schalkwyk, L. C., Rastan, S., Brown, S. D., Bussow, K., Himmelbauer, H., and Lehrach, H. (2002) *Nat Genet* **30**, 385-393
3. Voss, T., Ahorn, H., Haberl, P., Dohner, H., and Wilgenbus, K. (2001) *Int J Cancer* **91**, 180-186
4. Moch, H., Schraml, P., Bubendorf, L., Mirlacher, M., Kononen, J., Gasser, T., Mihatsch, M. J., Kallioniemi, O. P., and Sauter, G. (1999) *Am J Pathol* **154**, 981-986
5. Celis, J. E., Celis, P., Ostergaard, M., Basse, B., Lauridsen, J. B., Ratz, G., Rasmussen, H. H., Orntoft, T. F., Hein, B., Wolf, H., and Celis, A. (1999) *Cancer Res* **59**, 3003-3009

6. Golub, T. R., Slonim, D. K., Tamayo, P., Huard, C., Gaasenbeek, M., Mesirov, J. P., Coller, H., Loh, M. L., Downing, J. R., Caligiuri, M. A., Bloomfield, C. D., and Lander, E. S. (1999) *Science* **286**, 531-537
7. Dang, C. V., Lewis, B. C., Dolde, C., Dang, G., and Shim, H. (1997) *J Bioenerg Biomembr* **29**, 345-354
8. Lee, W. N., Bassilian, S., Guo, Z., Schoeller, D., Edmond, J., Bergner, E. A., and Byerley, L. O. (1994) *Am J Physiol* **266**, E372-383
9. Wittmann, C., and Heinzle, E. (1999) *Biotechnol Bioeng* **62**, 739-750
10. Delaglio, F., Grzesiek, S., Vuister, G. W., Zhu, G., Pfeifer, J., and Bax, A. (1995) *J Biomol NMR* **6**, 277-293
11. Szyperski, T. (1995) *Eur J Biochem* **232**, 433-448
12. Gribbestad, I. S., Petersen, S. B., Fjosne, H. E., Kvinnsland, S., and Krane, J. (1994) *NMR Biomed* **7**, 181-194
13. Gribbestad, I. S., Sitter, B., Lundgren, S., Krane, J., and Axelson, D. (1999) *Anticancer Res* **19**, 1737-1746
14. Pal, K., Sharma, U., Gupta, D. K., Pratap, A., and Jagannathan, N. R. (2005) *Spine* **30**, E68-72
15. Patel, A. B., Srivastava, S., Phadke, R. S., and Govil, G. (1999) *Anal Biochem* **266**, 205-215
16. Sharma, U., Atri, S., Sharma, M. C., Sarkar, C., and Jagannathan, N. R. (2003) *NMR Biomed* **16**, 213-223
17. Sharma, U., Mehta, A., Seenu, V., and Jagannathan, N. R. (2004) *Magn Reson Imaging* **22**, 697-706
18. Dauner, M., Bailey, J. E., and Sauer, U. (2001) *Biotechnol Bioeng* **76**, 144-156
19. Schmidt, K., Nielsen, J., and Villadsen, J. (1999) *J Biotechnol* **71**, 175-189
20. Fernandez, C. A., and Des Rosiers, C. (1995) *J Biol Chem* **270**, 10037-10042
21. Lapidot, A., and Gopher, A. (1994) *J Biol Chem* **269**, 27198-27208
22. Jeffrey, F. M., Storey, C. J., Sherry, A. D., and Malloy, C. R. (1996) *Am J Physiol* **271**, E788-799
23. Malloy, C. R., Sherry, A. D., and Jeffrey, F. M. (1988) *J Biol Chem* **263**, 6964-6971
24. Vercoutere, B., Durozard, D., Baverel, G., and Martin, G. (2004) *Biochem J* **378**, 485-495
25. Lu, D., Mulder, H., Zhao, P., Burgess, S. C., Jensen, M. V., Kamzolova, S., Newgard, C. B., and Sherry, A. D. (2002) *Proc Natl Acad Sci U S A* **99**, 2708-2713
26. Cline, G. W., Lepine, R. L., Papas, K. K., Kibbey, R. G., and Shulman, G. I. (2004) *J Biol Chem* **279**, 44370-44375
27. Boren, J., Cascante, M., Marin, S., Comin-Anduix, B., Centelles, J. J., Lim, S., Bassilian, S., Ahmed, S., Lee, W. N., and Boros, L. G. (2001) *J Biol Chem* **276**, 37747-37753
28. Boren, J., Lee, W. N., Bassilian, S., Centelles, J. J., Lim, S., Ahmed, S., Boros, L. G., and Cascante, M. (2003) *J Biol Chem* **278**, 28395-28402
29. Portais, J. C., Schuster, R., Merle, M., and Canioni, P. (1993) *Eur J Biochem* **217**, 457-468
30. Boros, L. G., Cascante, M., and Lee, W. N. (2002) *Drug Discov Today* **7**, 364-372
31. Baron, A., Migita, T., Tang, D., and Loda, M. (2004) *J Cell Biochem* **91**, 47-53
32. Meister, A. (1991) *Pharmacol Ther* **51**, 155-194